Eur. Phys. J. D **37**, 29–35 (2006)
DOI: 10.1140/epjd/e2005-00256-8

THE EUROPEAN PHYSICAL JOURNAL D

Radiative lifetimes and transition probabilities in Ta I

V. Fivet[1], P. Palmeri[1], P. Quinet[1,2], É. Biémont[1,2,a], H.L. Xu[3], and S. Svanberg[3]

[1] Astrophysique et Spectroscopie, Université de Mons-Hainaut, 15 rue de la Halle, 7000 Mons, Belgium
[2] IPNAS (Bât. B15), Université de Liège, 4000 Liège, Belgium
[3] Department of Physics, Lund Institute of Technology, P.O. Box 118, 22100 Lund, Sweden

Received 23 June 2005 / Received in final form 10 August 2005
Published online 20 September 2005 –

Abstract. Radiative lifetimes of 14 odd-parity Ta I levels, belonging to the $5d^3 6s6p$ and $5d^4 6p$ configurations in the energy range from 30 664 to 45 256 cm^{-1}, have been measured using the time-resolved laser-induced fluorescence technique. Extensive calculations, taking configuration interactions and core-polarisation effects into account, are able to reproduce in a satisfying way the available experimental results but suffer from the rather fragmentary knowledge of the level structure of this atom. New transition probabilities are deduced for a set of strong lines depopulating the levels investigated experimentally in the present work.

PACS. 31.25.-v Electron correlation calculations for atoms and molecules – 52.38.-r Laser-plasma interactions

1 Introduction

The investigation of the radiative properties of the heavy elements, particularly those of the sixth row of the periodic table (from Hf to Rn), is a very complex task both theoretically and experimentally. The recent registration with the Hubble Space Telescope of a large number of astrophysical spectra, characterized by a high resolution and a high signal-over-noise ratio, requires extensive atomic data for their interpretation (see e.g. [1,2]). Such data (levels, radiative lifetimes, transition probabilities, hyperfine structure constants, ...) allow a determination of the chemical composition of the stars and, consequently, are useful for nucleosynthesis and cosmochronology.

Experimental investigations of heavy refractory elements are difficult due to the low vapour pressure produced by sputtering from cathode discharges or by laser-produced plasmas. In addition, experiments to measure oscillator strengths are often hampered by the lack of knowledge of the term structure of these elements, or by misidentifications of spectral lines or levels in previous publications.

The atomic structure of heavy elements is also difficult to calculate accurately as the models must include both relativity and correlation effects because most of the spectra of the group are strongly perturbed. An additional difficulty results from the structural complexity associated with the progressive filling, along the period, of the $5d$ shell (up to gold) and of the $6p$ shell (up to radon).

For these reasons, we have concentrated in this work on neutral tantalum (Ta I), an element with "moderate" complexity, the ground configuration being $5d^3 6s^2$. During the past few years, there have been several analyses of the atomic structure (see e.g. [3,4]) and hyperfine structure (see e.g. [5–8]) of Ta I but little has been done concerning the transition probabilities or radiative lifetimes determination.

An additional motivation of the present work results from potential application of the results to astrophysics. It does appear, for example, that the photospheric abundance of tantalum is still unknown. Singly ionized tantalum, Ta II, has been looked for but has not been detected in the CP star χ Lupi star (see [1]) and the neutral atom, Ta I, has been also investigated in stellar spectra (see e.g. [9,10]). In stellar nucleosynthesis, it is expected that the elements of the sixth period will play an important role in relation with the rapid (r) and slow (s) processes (neutron captures) occurring in stellar atmospheres.

2 Previous work

Tantalum has two stable isotopes ^{180}Ta and ^{181}Ta and 16 short-lived isotopes and isomers. In the solar system, ^{181}Ta is by far the dominant species (99.988%). For ^{181}Ta $I = 7/2$ and, consequently, the spectrum of this element is strongly affected by hyperfine structure (see e.g. [6,11,12] for recent references).

The energy levels published in the NBS compilation [13] were deduced from different analyses due to Kiess and Kiess [14–16] and to Klinkenberg et al. [17,18], Van den Berg et al. [19] and Van Kleef and Klinkenberg [20]. More recent results concerning the analysis of the spectrum of Ta I are due to Dembczynski et al. [3], Guthöhrlein

[a] e-mail: e.biemont@ulg.ac.be

et al. [4,21], Berzinsh et al. [22], Persson et al. [23] and Windholz and Guthöhrlein [5]. A complete list of the observed Ta I and Ta II spectral lines and of the existing energy levels can be downloaded from the site: `http://iep.tu-graz.ac.at/ta.html`. Many references about recent work on hyperfine structure of this element (not considered in the present paper) can be found also on the same site.

Transition probabilities or radiative lifetimes in Ta I are rather sparse. The first published work summarizes the arc measurements of Corliss and Bozman [24]. Spectrometric investigations of an inductively coupled plasma are due to Jarosz et al. [25] who published oscillator strengths for 14 transitions. More recently, radiative lifetimes were reported for 35 levels of Ta I [26]. Branching fraction measurements were performed also at the University of Wisconsin for 253 spectral lines in Ta I [27]. From a combination of the lifetimes and branching fractions, these authors were able to produce a new set of transition probabilities [27]. A compilation of oscillator strengths for the resonance transitions of heavy elements published by Morton [28] includes the Ta I data.

3 Experimental lifetimes

A useful method for the determination of transition probabilities consists in combining measured radiative lifetimes (obtained by laser spectroscopy) with experimental (measured e.g. with a Fourier transform spectrometer) or theoretical (calculated by different theoretical approaches) branching fractions (BF). As the measured BFs are available generally for a limited number of transitions, theoretical data are frequently the only way to get the required transition probabilities. The theoretical approach does allow also an estimation of the missing branches appearing in the far UV or infrared regions where measurements are sometimes difficult.

In the present work, radiative lifetime measurements were performed using a time-resolved laser-induced fluorescence (LIF) technique, which is among the most reliable methods available for lifetime measurements. In this approach, the levels of interest in Ta I were selectively excited and the fluorescence emitted from the investigated levels was subsequently monitored by a fast detection system. The method has been extensively described previously (see e.g. [29–31]) and, consequently, we recall here only the details specific to the Ta experiment.

The tantalum atoms were generated in a laser-produced plasma by focusing the pulse from a 532 nm Nd:YAG laser (Continuum Surelite) onto a rotating tantalum target. The pulse energy was normally used in the range of 1−5 mJ. The excitation pulses have a duration of about 1 ns. This was achieved by sending a frequency-doubled Nd:YAG laser (Continuum NY-82) pulse into a temporal compressor, which is based on stimulated Brillouin scattering (SBS) technique in water [29]. The Nd:YAG laser consists of an injection seeding system, which results in a pulsed output with a single longitudinal mode and improves significantly the laser energy stability. In order to generate the required excitation wavelengths, the compressed pulses were used to pump a dye laser (Continuum Nd-60). Using the DCM dye, the region of the required excitation wavelengths can be covered by different non-linear processes, such as frequency upconversion in crystals (KDP and BBO) and stimulated Raman scattering in a hydrogen gas cell (10 bar). The Raman scattering components include 2ω, $2\omega+A$, $3\omega+2S$ and $3\omega+S$, where 2ω and 3ω designate the second and third harmonics of the dye laser, A, S and $2S$ represent the first-order anti-Stokes and the first- and second-order Stokes components. The appropriate frequency component of the output from the H_2 cell was selected with a CaF_2 prism, and was then horizontally sent into a vacuum chamber where the tantalum foil was located. The excitation beam interacted with the neutral tantalum atoms about 1 cm above the foil.

This technique has several advantages. The first is that it can produce free tantalum atoms in the ground and metastable states, giving access to a larger number of levels than possible if only the ground term is excited. The second one is that the plasma density and temperature can be easily controlled and adjusted by changing the pulse energy, the beam size on the foil, and also the delay time between the ablation and the excitation pulses. The third one is that, since the delay time between the ablation and excitation pulses can be easily controlled and since the speed of the ions is different from that of the atoms, the excitation pulses can be applied only to the atoms by selecting appropriate delay times [29,32,33].

The fluorescence emitted from the excited levels was collected by a fused-silica lens and focused onto the entrance slit of a 1/8 m monochromator (resolution of 6.4 nm/mm). It was then detected by a Hamamatsu 1564U micro-channel-plate (MCP) photomultiplier tube (PMT), which had a risetime of 0.2 ns. The MCP PMT was connected to a transient recorder (Tektronix Model DSA 602) with a real-time sampling rate of 2 G samples/s. It is necessary to record the shape of the excitation pulses in order to measure short lifetimes accurately using the same detection system. The sample was placed in a vacuum chamber with a background pressure of 10^{-6}−10^{-5} mbar. The excitation process was also produced in this vacuum chamber. For more details, see [29,34].

Radiative lifetimes of 14 odd-parity Ta I levels were measured, belonging to the $5d^36s6p$ and $5d^46p$ configurations in the energy range from 30 664 to 45 256 cm^{-1}. The fluorescence signals of the different decay channels from the excited upper level to possible lower levels were checked in order to avoid a wrong choice of a level. The channels having the stronger signals were normally retained for the decay recordings. The relevant information on the levels, on the excitation schemes and on the corresponding observed wavelengths is collected in Table 1 together with the new and previously measured radiative lifetimes. In some cases (see column 7), fluorescence decays were measured using two different wavelengths but it was verified that the corresponding lifetimes were in agreement within the error bars.

Table 1. Measured lifetimes in Ta I.

Config.[a]	Term[a]	J	E (cm^{-1})	Origin[b]	Exc.[c]	Obs[d]	τ (ns)	
					λ(nm)	λ(nm)	This work	Previous[e]
$5d^3 6s(^5\mathrm{P})6p$	$^6\mathrm{D}^0$	1.5	30 664.66	0.0	326.11	406	58(4)	57.9(3.0)
		3.5	34 094.66	2 010.10	311.68	351, 482	47(4)	
	$^6\mathrm{P}^0$	1.5	31 066.34	0.0	321.89	400, 469	53(4)	54.0(2.7)
		2.5	31 961.42	0.0	312.88	334	82(7)	81.7(4.1)
$5d^3 6s(^3\mathrm{H})6p$	$^4\mathrm{G}^0$?	2.5	36 013.97	0.0	277.67	334, 399	17.5(1.5)	
		3.5	36 799.88	5 621.04	320.73	363, 391	40(4)	
	$^4\mathrm{H}^0$?	3.5	36 159.13	5 621.04	327.46	293, 378	12.7(1.2)	
$5d^3 6s(^3\mathrm{G})6p$	$^4\mathrm{F}^0$?	1.5	36 580.06	0.0	273.37	403	15.5(1.5)	
$5d^4(^5\mathrm{D})6p$	$^6\mathrm{F}^0$	0.5	38 507.54	0.0	259.69	308, 348	7.5(0.4)	
		2.5	41 580.98	0.0	240.49	282, 309	5.6(0.3)	
	$^4\mathrm{P}^0$	0.5	43 478.20	0.0	230.00	267, 316	8.2(0.5)	
	$^6\mathrm{P}^0$	1.5	45 241.73	2 010.10	231.31	221, 299	4.8(0.3)	
	$^6\mathrm{D}^0$	1.5	45 246.22	2 010.10	231.29	255, 299	4.9(0.3)	
		2.5	45 255.98	2 010.10	231.24	309, 291	4.3(0.2)	

[a] Reference [13]. [b] Starting level for the excitation. [c] Wavelength of the excitation. [d] Wavelength of the fluorescence decay. [e] Reference [26]. $a(b)$ is written for $a \pm b$.

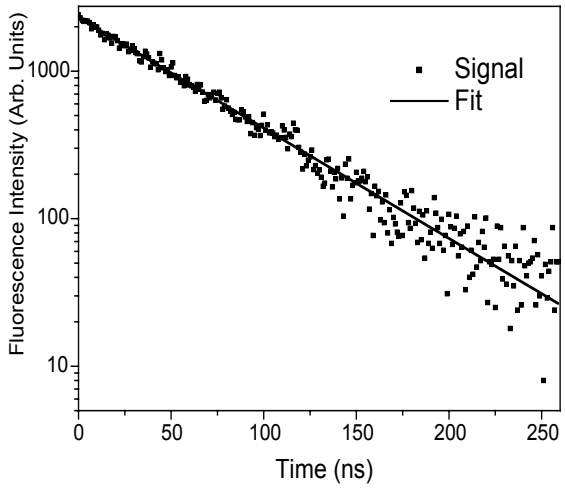

Fig. 1. A typical Ta I experimental decay curve with an exponential fit. The lifetime for this level, situated at 30 664.66 cm^{-1}, is 58 ± 4 ns.

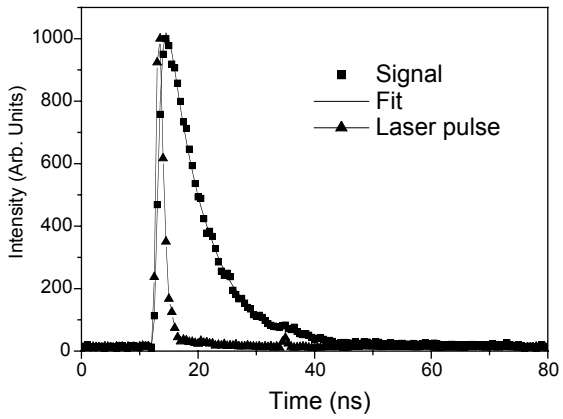

Fig. 2. Detected time-resolved fluorescence signal from the level at 41 580.98 cm^{-1} in Ta I and the recorded excitation laser pulse. The convolution procedure gives a lifetime of 5.6 ± 0.3 ns.

As shown in Table 1, the measured lifetime values fall in the range 4−85 ns. For the $5d^3 6s6p$ configuration, the fluorescence lifetimes obtained are longer than 10 ns. In this case, the impact of the temporal shape of the excitation pulse could be eliminated by applying an exponential fitting procedure to the decay curve after some delay following the excitation pulse. Figure 1 shows the fluorescence signal (rectangle) of the $5d^3 6s(^5\mathrm{P})6p\ ^6\mathrm{D}^0_{3/2}$ level and its exponential fitting plot (solid line) in a semi-logarithmic representation. The fit gives a lifetime of 58 ± 4 ns, which is in good agreement with the previous result, 57.9 ± 3.0 ns, obtained by Salih et al. [26] using the LIF technique, but with a hollow cathode lamp as a source. For the $5d^4 6p$ configuration, on the other hand, the lifetimes obtained are shorter than 10 ns and, consequently, the temporal shape of the excitation pulse has to be taken into account during the fitting procedure. The evaluation process was performed by fitting the experimental fluorescence decay curve to a convolution of the recorded excitation pulse and a pure exponential function. A typical convolution curve (solid line) is shown in Figure 2 together with the time-resolved signal (rectangle) and the excitation pulse (triangle).

Several possible systematic error sources have been taken into account during the measurements, by varying the experimental parameters. To check collisional quenching and radiative trapping, the intensity of the ablation pulse and the delay time between the excitation and the ablation pulses were changed. Although the signal

Table 2. List of configurations used in the present calculations. The underlined configurations have been investigated experimentally by Van den Berg et al. [19].

Even parity	Odd parity
$\underline{5d^3 6s^2}$	$\underline{5d^4 6p}$
$\underline{5d^4 6s}$	$5d^4 7p$
$5d^4 7s$	$\underline{5d^3 6s 6p}$
$5d^4 6d$	$5d^3 6s 7p$
$5d^5$	$5d^3 6s 5f$
$5d^3 6p^2$	$5d^3 6s 6f$
$\underline{5d^3 6s 7s}$	$\underline{5d^2 6s^2 6p}$
$5d^3 6s 6d$	$5d^2 6s^2 5f$
$5d^2 6s^2 6d$	$5d^2 6s^2 6f$
$5d^2 6s 6p^2$	

intensities were dramatically changed, the lifetime values were found to be constant within the statistical error bars, which implied that collisions and radiation trapping effects were negligible [30]. Different neutral density filters, inserted in the exciting light path, were used to avoid the saturation effects. Long delay times (10 μs) between the ablation and excitation pulses were also adopted to minimize the possible flight-out-of-view effects. A static magnetic field of about 100 Gauss, provided by a pair of Helmholtz coils, was applied to the laser-induced plasma in order to check for possible Zeeman quantum-beats effects. No observable effects were found. For a more detailed discussion, see references [30,33].

The final lifetime of each level was obtained by averaging a number of recordings under different experimental conditions. The error bars of the values in Table 1 were determined from statistical uncertainties associated with the different curve recordings. As can been seen from Table 1, besides the $5d^3 6s(^5\mathrm{P})6p\ ^6\mathrm{D}^0_{3/2}$ level, the $5d^3 6s(^5\mathrm{P})6p\ ^6\mathrm{P}^0_{3/2}$ and the $5d^3 6s(^5\mathrm{P})6p\ ^6\mathrm{P}^0_{5/2}$ levels have also been measured previously with the method of LIF combined with a hollow cathode discharge lamp by Salih et al. [26]. Our results, 53 ± 4 and 82 ± 7 ns, agree very well with the previous values i.e. 54.0 ± 2.7 and 81.7 ± 4.1 ns.

4 HFR calculations

The calculations reported in the present work have been performed with the Cowan code [35] modified for the inclusion of core-polarisation effects (Relativistic Hartree-Fock or HFR approach) [36]. The configurations considered in the calculations are reported in Table 2, the underlined configurations having been observed by Van den Berg et al. [19]. A scaling factor of 0.80 was applied to the F^k, G^k et R^k integrals according to a well-established procedure [35] and the spin-orbit integrals were kept at their ab initio values.

A least-squares fitting procedure was applied in order to better adjust the calculated eigenvalues to the observed energy levels. The energy levels were

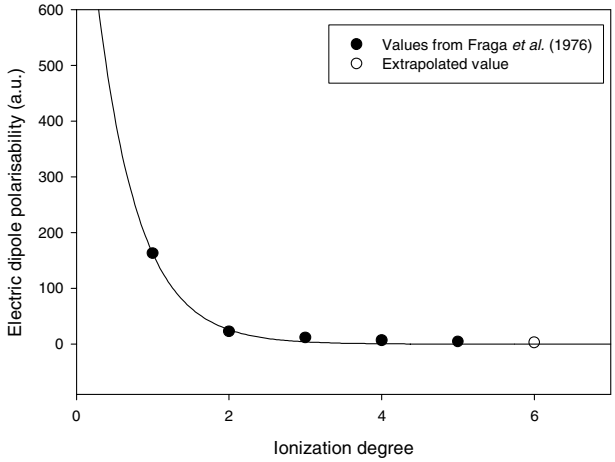

Fig. 3. Electric dipole polarisability vs. the ionisation stage. Filled circles: Fraga et al. [40]; open circle: extrapolated value.

taken from the compilation available from the web site: `http://iep.tu-graz.ac.at/ta.html` which incorporates levels from recent term analyses [4,37,38]. The "non-existing" levels mentioned in reference [11] (see Tab. V in that paper) were excluded from the fit. This is the case particularly for the low-lying levels at 14 875.70 cm^{-1}, 21 091.53 cm^{-1} and 22 434.37 cm^{-1}, respectively, which appear in Moore's [13] compilation. This is the case also for the low-lying level at 11 796.14 cm^{-1}, previously identified as $5d^5\ ^6\mathrm{S}_{5/2}$ but which was calculated at a much higher energy (at about 31 700 cm^{-1}) in agreement with a systematic analysis of the $5d^N$ configuration for the platinum group elements [39].

In the fitting procedure (due to space limitations, the details of the fitting procedure are not reproduced in the present paper), the high odd energy levels available (above 38 000 cm^{-1}) could not be included in the calculations because many of them are not labeled in relation with the strong mixing occurring at high energies. An unambiguous connection between experimental and calculated level values could not be established even when using the experimental values available for the Landé factors. The mean deviation in the fit was 140 cm^{-1} for the even parity (28 levels) and 266 cm^{-1} for the odd parity (106 levels).

Core-polarisation was introduced in the calculations in two different ways. In the first model, all the shells up to $5p$ were considered as part of the ionic core while, in the second one, the shells up to $5d$ were retained as such. The values of the static dipole polarisability were taken from Fraga et al. [40]. For the $5p$ model, we had to extrapolate the polarisability curve as a function of the ionisation stage for higher ionisation charges as illustrated in Figure 3. We have adopted $\alpha_{5d} = 6.75$ a.u. and $\alpha_{5p} = 2.81$ a.u. The values of the cut off radius were chosen as $\langle r \rangle_{5d} = 2.20$ a.u. and $\langle r \rangle_{5p} = 1.31$ a.u.

The lifetimes calculated with the two models are reported in Table 3 where they are compared with the experimental measurements of Salih et al. [26].

Table 3. Comparison of experimental lifetimes (τ in ns) calculated with two core-polarisation models with experimental values.

Config.[c]	Term[c]	J	Obs. level (cm^{-1})	τ_{exp} [d]	τ_{exp} [e]	τ_{theory} This work, Pol. $5d$	τ_{theory} This work, Pol. $5p$
$5d^26s^2(^3F)6p$	$^4D^0$	1/2	18 504.72	572		443	433
$5d^26s^2(^3P)6p$	$^2D^0$	3/2	20 772.32	685		604	444
$5d^26s^2(^3F)6p$	$^4D^0$	5/2	21 167.61	908		555	512
$5d^36s(^5F)6p$	$^4F^0$	3/2	21 855.07	449		460	353
$5d^36s(^5F)6p$	$^4F^0$	5/2	23 363.09	390		520	366
$5d^36s(^5F)6p$	$^6D^0$	3/2	24 739.03	170		204	163
$5d^36s(^5F)6p$	$^4D^0$	1/2	25 512.63	112		170	124
$5d^36s(^5F)6p$	$^4D^0$	3/2	26 363.69	128		111	91
$5d^36s(^5F)6p$	$^6F^0$	7/2	26 585.93	261		312	250
$5d^36s(^3P)6p$	$^4P^0$?	3/2	26 590.03	176		339	250
$5d^36s(^5F)6p$	$^6D^0$	5/2	26 794.76	113		183	151
unclassified		7/2	26 960.46	285		438	336
$5d^36s(^5F)6p$	$^6F^0$	9/2	27 733.43	265		314	255
$5d^36s(^5F)6p$	$^6D^0$?	7/2	27 780.62	120		111	91
unclassified		11/2	27 783.0?	379		343	300
$5d^36s(^5F)6p$	$^4D^0$	5/2	28 133.88	157		190	148
unclassified		3/2	28 689.31	138		183	142
$5d^36s(^5F)6p$	$^6D^0$?	9/2	28 766.65	138		152	127
unclassified		5/2	28 862.01	180		371	283
unclassified		5/2	29 343.46	97.5		258	213
unclassified		7/2	29 722.95	129		187	149
unclassified		9/2	30 021.20	238		260	211
$5d^36s(^5F)6p$	$^6F^0$?	11/2	30 361.22	304		338	272
unclassified		7/2	30 590.95	139		290	237
$5d^36s(^5P)6p$	$^6D^0$	3/2	30 664.66	57.9	58(4)	52	43
$5d^36s(^5P)6p$	$^4S^0$	3/2	30 894.67	75.4		165	134
$5d^36s(^5P)6p$	$^6P^0$	3/2	31 066.34	54	53(4)	46	36
unclassified		9/2	31 530.02	122		193	163
unclassified		3/2	31 553.89	97.1		217	164
unclassified		7/2	31 600.95	106		153	121
$5d^36s(^5P)6p$	$^6P^0$	5/2	31 961.42	81.7	82(8)	61	50
$5d^36s(^5P)6p$	$^6D^0$	5/2	32 486.75	60.5		85	70
unclassified		11/2	33 070.28	175		220	186
$5d^36s(^5P)6p$	$^6P^0$	7/2	33 197.75	63.4		60	49
unclassified		9/2	33 497.15	54.3		70	62
$5d^36s(^5P)6p$	$^6D^0$	7/2	34 094.66		47(4)	60	50
$5d^36s(^3H)6p$	$^4G^0$?	5/2	36 013.97		17.5(1)	19.1	15.9
$5d^36s(^3H)6p$	$^4H^0$?	7/2	36 159.13		12.7(1.2)	-	-
$5d^36s(^3G)6p$	$^4F^0$?	3/2	36 580.06		15.5(1.5)	10.7	8.8
$5d^36s(^3H)6p$	$^4G^0$?	7/2	36 799.88		40(4)	40	34
$5d^4(^5D)6p$	$^6F^0$	1/2	38 507.54		7.5(0.4)	7.5	6.5
$5d^4(^5D)6p$	$^6F^0$	5/2	41 580.98		5.6(0.3)	4.8	4
$5d^4(^5D)6p$	$^4P^0$	1/2	43 478.20		8.2(0.5)	-	-
$5d^4(^5D)6p$	$^6P^0$	3/2	45 241.73		4.8(0.4)	4.6	4
$5d^4(^5D)6p$	$^6D^0$	3/2	45 246.22		4.9(0.2)	4.4	3.8
$5d^4(^5D)6p$	$^6D^0$	5/2	45 255.98		4.3(0.2)	3.3	2.9

$a(b)$ is written for $a \pm b$. [c]Reference [13]. The experimental results are due to Salih et al. [26] [d] or have been measured at Lund (present work) [e].

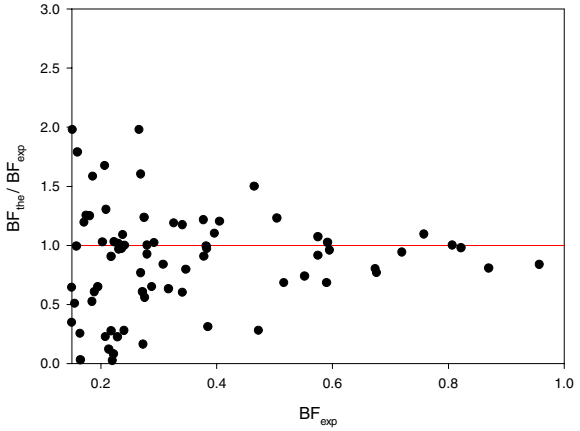

Fig. 4. Comparison between theoretical and experimental branching fractions. The ratio between theoretical and experimental BFs is plotted vs. the experimental BFs [26].

5 Results and discussion

It does appear, from Table 3, that the lifetimes obtained with the $5p$ model are generally smaller than those derived with the $5d$ model. A better agreement with experiment is observed with the $5d$ model in the case of the small lifetime values while this is much less obvious when the lifetimes are longer.

No theoretical lifetimes are provided in Table 3 for the two levels at 36 159.13 cm^{-1} and 43 478.20 cm^{-1} because it was impossible to establish an unambiguous connection between the calculated and observed levels values. These two levels have not been deduced experimentally by Van den Berg et al. [19] but have been quoted in Moore's [13] compilation.

It is seen that, in a general way, the agreement between theory and experiment is satisfying. Large discrepancies are observed, however, for a number of levels. They are probably due to the theoretical data because the lifetime measurements of Salih et al. [26] were obtained also by time-resolved laser-induced fluorescence and agree well with the present measurements. Although some uncertainties in the branching fraction measurements cannot be ruled out, particularly for the weak transitions, it is more plausible to believe that the largest part of the discrepancies is originating from the theoretical values. Possible explanations are the limited amount of configuration interaction included in the calculations (although this is partly corrected by the scaling down of the Slater integrals) but also the fact that some levels are depopulated through channels which are affected by cancellation effects. These deexcitation transitions are characterized by very small transition probabilities inducing too large values for the lifetimes, which is indeed the case for a number of levels.

It is interesting to compare the theoretical branching fractions with those obtained experimentally by Den Hartog et al. [27]. The comparison is shown in Figure 4. As expected, the largest discrepancies are observed for the weak lines. The mean value of the ratio (BF_{th}/BF_{exp}) is 0.891 ± 0.278 if $BF \geq 0.2$, 0.914 ± 0.194 if $BF \geq 0.3$ and 0.922 ± 0.188 if $BF \geq 0.4$. This indicates an uncertainty on the theoretical branching fractions of a few, up to 20%, for the strong transitions.

Table 4. New theoretical branching fractions (BF) and weighted transition probabilities (gA) for the transitions depopulating the levels for which lifetimes have been measured in the present work. The transitions are listed in order of increasing upper level energies.

λ obs. (nm)	Lower level[a] (cm^{-1})	Upper level[a] (cm^{-1})	gA (NORM)[b] (s^{-1})	BF (HFR)[c] (%)
311.59	2 010.10	34 094.66	2.66×10^7	15.7
331.79	3 963.92	34 094.66	4.89×10^7	28.9
351.10	5 621.04	34 094.66	4.51×10^7	26.7
481.95	13 351.45	34 094.66	3.05×10^7	18.0
277.59	0	36 013.97	2.17×10^8	63.4
650.55	20 646.54	36 013.97	3.81×10^7	11.1
289.18	2 010.10	36 580.06	2.25×10^8	87.0
382.89	10 690.32	36 799.88	2.89×10^7	14.4
638.94	21 153.33	36 799.88	9.42×10^7	46.9
308.18	6 068.91	38 507.54	9.97×10^7	37.5
347.74	9 758.97	38 507.54	3.82×10^7	14.4
350.39	9 975.81	38 507.54	1.10×10^8	41.4
252.64	2 010.10	41 580.98	2.72×10^8	25.2
309.24	9 253.43	41 580.98	2.50×10^8	23.1
340.66	12 234.76	41 580.98	2.36×10^8	21.9
255.08	6 049.42	45 241.73	3.92×10^8	46.7
291.53	10 950.22	45 241.73	1.16×10^8	13.8
281.71	9 758.97	45 246.22	3.81×10^8	46.6
283.44	9 975.81	45 246.22	1.00×10^8	12.2
255.10	6 068.91	45 255.98	2.94×10^8	21.3
283.36	9 975.81	45 255.98	1.77×10^8	12.8
291.41	10 950.22	45 255.98	2.25×10^8	16.3
302.75	12 234.76	45 255.98	3.49×10^8	25.2

[a]Reference [13]. [b]NORM: results obtained from the experimental lifetimes of this work and the HFR BFs. [c]HFR: results calculated with the HFR method ($5d$ polarisation model: see the text).

We report in Table 4 the BFs and the corresponding transition probabilities (derived from the experimental lifetime values and the theoretical BFs) for the strongest transitions depopulating the levels for which radiative lifetimes have been measured in the present work and for which no data were previously available. It is expected that these values are also accurate to a few ($\leq$20)%.

We have tentatively applied the transition probabilities obtained in the present work to a determination of the solar abundance of tantalum which presently is still unknown [41], the meteoritic abundance being well-known. We have considered a set of six transitions characterized by a small lower excitation potential (a fraction of eV), a large oscillator strength and which appear in an unblended region of the photospheric spectrum. Using the best available solar model [42] and new partition functions calculated on the basis of the available energy levels in Ta I and

Ta II, it does appear that the contribution of Ta I to the observed solar features is too weak by about a factor 100 to be observable. This is in agreement with the fact that Ta II is expected to be the dominant species in the solar photosphere according to Saha equation. An investigation of Ta II transitions, similar to the one carried out in the present work, would therefore be extremely useful.

This work was financially supported by the Swedish Research Council and by the EU-TMR access to Large-Scale Facility Programme (contract RII3-CT-2003-506350). Financial support from the Belgian FNRS is acknowledged by two of us (E.B. and P.Q.) who are, respectively, Research Director and Research Associate of the Belgian FNRS. P.P. was funded by a return grant of the Belgian Federal Science Policy.

References

1. M. Eriksson, U. Litzén, G.M. Wahlgrén, D.S. Leckrone, Phys. Scripta **65**, 480 (2002)
2. D.S. Leckrone, C.R. Proffitt, G.M. Wahlgren, S.G. Johansson, T. Brage, Astron. J. **117**, 1454 (1999)
3. J. Dembczynski, B. Arcimowicz, G.H. Guthöhrlein, L. Windholz, Z. Phys. D **39**, 143 (1997)
4. G.H. Guthöhrlein, H. Mocnik, L. Windholz, Z. Phys. D **35**, 177 (1995)
5. L. Windholz, G.H. Guthöhrlein, Phys. Scripta T **105**, 55 (2003)
6. D. Messnarz, N. Jaritz, B. Arcimowicz, V.O. Zilio, R. Engleman Jr, J.C. Pickering, H. Jäger, G.H. Guthöhrlein, L. Windholz, Phys. Scripta **68**, 170 (2003)
7. H. Mocnik, B. Arcimowicz, W. Salmhofer, L. Windholz, G.H. Guthöhrlein, Z. Phys. D **36**, 129 (1996)
8. H. Hammerl, G.H. Guthöhrlein, M. Elantkovska, V. Funtov, G. Gwehenberger, L. Windholz, Z. Phys. D **33**, 97 (1995)
9. D.L. Lambert, in *Cool Stars with Excesses of Heavy Elements*, edited by M. Jaschek, P.C. Keenan (Reidel, 1985)
10. V.V. Smith, A&A **132**, 326 (1984)
11. N. Jaritz, L. Windholz, D. Messnarz, H. Jäger, R. Engleman Jr, Phys. Scripta **71**, 611 (2005)
12. N. Jaritz, G.H. Guthöhrlein, L. Windholz, D. Messnarz, R. Engleman Jr, J.C. Pickering, H. Jäger, Phys. Scripta **69**, 441 (2004)
13. C.E. Moore, *Atomic Energy Levels*, Vol. III, Circular **357** (National Bureau of Standards, Washington D.C., 1958)
14. C.C. Kiess, H.K. Kiess, J. Res. Nat. Bur. Stand. **11**, 277 (1933)
15. C.C. Kiess, H.K. Kiess, J. Opt. Soc. Am. **41**, 867 (1951)
16. C.C. Kiess, H.K. Kiess, Unpublished material (1957)
17. P.F.A. Klinkenberg, G.J. Van den Berg, J.C. Van den Bosch, Physica **16**, 861 (1950)
18. P.F.A. Klinkenberg, G.J. Van den Berg, J.C. Van den Bosch, Physica **17**, 167 (1951)
19. G.J. Van den Berg, P.F.A. Klinkenberg, J.C. Van den Bosch, Physica **18**, 221 (1952)
20. Th.A.M. Van Kleef, P.A. Klinkenberg, Phys. Rev. **101**, 489 (1956)
21. G.H. Guthöhrlein, G. Helmrich, L. Windholz, Phys. Rev. A **49**, 120 (1994)
22. U. Berzinsh, M. Gustafsson, J. Persson, Z. Phys. D **27**, 155 (1993)
23. J. Persson, U. Berzinsh, T. Nilsson, M. Gustavsson, Z. Phys. D **23**, 67 (1992)
24. C.H. Corliss, W.R. Bozman, NBS, Monograph **53** (US Department of Commerce, Washington D.C., 1962)
25. J. Jarosz, J.M. Mermet, J. Robin, Spectrochim. Acta B **33**, 365 (1978)
26. S. Salih, D.W. Duquette, J.E. Lawler, Phys. Rev. A **27**, 1193 (1983)
27. E.A. Den Hartog, D.W. Duquette, J.E. Lawler, J. Opt. Soc. Am. B **4**, 48 (1987)
28. D.C. Morton, Astrophys. J. Suppl. Ser. **130**, 403 (2000); D.C. Morton, Astrophys. J. Suppl. Ser. **132**, 411 (2001)
29. H.L. Xu, A. Persson, S. Svanberg, K.B. Blagoev, G. Malcheva, V. Penchev, É. Biémont, Phys. Rev. A **70**, 042508 (2004)
30. H.L. Xu, S. Svanberg, P. Quinet, H.P. Garnir, É. Biémont, J. Phys. B **36**, 4773 (2003)
31. H.L. Xu, S. Svanberg, R.D. Cowan, P.-H. Lefèbvre, P. Quinet, É. Biémont, Mont. Not. Roy. Astron. Soc. **346**, 433 (2003)
32. H.L. Xu, A. Persson, S. Svanberg, Eur. Phys. J. D **23**, 233 (2003)
33. H.L. Xu, Z.K. Jiang, S. Svanberg, J. Phys. B **36**, 411 (2003)
34. É. Biémont, P. Quinet, S. Svanberg, H.L. Xu, J. Phys. B **37**, 1381 (2004)
35. R.D. Cowan, *The Theory of Atomic Structure and Spectra* (Univ. of California, Berkeley, 1981)
36. P. Quinet, P. Palmeri, É. Biémont, M.M. McCurdy, G. Rieger, E.H. Pinnington, M.E. Wickliffe, J.E. Lawler, Mon. Not. R. Astron. Soc. **307**, 934 (1999)
37. N. Jaritz, D. Messnarz, R. Engleman Jr, H. Jäger, G. Guthörlein, L. Windholz, in Europhysics Conference abstracts 27B, S.193 (2003)
38. A. Huss, L. Windholz, Europhysics Conference Abstracts 20D, 142, Abstract A4-68 (1996)
39. J.-F. Wyart, Phys. Scripta **18**, 87 (1978)
40. S. Fraga, J. Karwowski, K.M.S. Saxena, *Handbook of Atomic Data* (Elsevier, Amsterdam, 1976)
41. M. Asplund, N. Grevesse, A.J. Sauval, In *Cosmic Abundances as Records of Stellar Evolution and Nucleosynthesis*, edited by F.N. Bash, T.G. Barnes (ASP Conf. Ser., San Francisco, in press, 2005)
42. H. Holweger, E.A. Müller, Solar Phys. **39**, 19 (1974)